

# SCIENTIFIC REPORTS



OPEN

## Directional Phonon Suppression Function as a Tool for the Identification of Ultralow Thermal Conductivity Materials

Giuseppe Romano & Alexie M. Kolpak

Received: 06 October 2016

Accepted: 07 February 2017

Published: 24 March 2017

Boundary-engineering in nanostructures has the potential to dramatically impact the development of materials for high-efficiency conversion of thermal energy directly into electricity. In particular, nanostructuring of semiconductors can lead to strong suppression of heat transport with little degradation of electrical conductivity. Although this combination of material properties is promising for thermoelectric materials, it remains largely unexplored. In this work, we introduce a novel concept, the directional phonon suppression function, to unravel boundary-dominated heat transport in unprecedented detail. Using a combination of density functional theory and the Boltzmann transport equation, we compute this quantity for nanoporous silicon materials. We first compute the thermal conductivity for the case with aligned circular pores, confirming a significant thermal transport degradation with respect to the bulk. Then, by analyzing the information on the directionality of phonon suppression in this system, we identify a new structure of rectangular pores with the same porosity that enables a four-fold decrease in thermal transport with respect to the circular pores. Our results illustrate the utility of the directional phonon suppression function, enabling new avenues for systematic thermal conductivity minimization and potentially accelerating the engineering of next-generation thermoelectric devices.

Understanding heat transport in the presence of nanoscale boundaries is of paramount significance for many applications, including thermoelectrics<sup>1,2</sup>, thermal rectifiers<sup>3</sup> and thermal dissipators<sup>4</sup>. When the dominant phonon mean free path (MFP)  $\Lambda$  approaches the characteristic length scale  $L_c$  of a material, classical phonon size effects lead to a decrease in thermal transport<sup>5</sup>. This regime is effectively described by the Knudsen number, defined as the ratio  $Kn = \Lambda/L_c$ . For example, first-principles calculations of silicon show that half of the heat is carried by phonons with MFPs larger than one micron<sup>6,7</sup>, supporting the strong phonon suppression observed in porous materials with microscale pores<sup>8</sup>. In addition, very low thermal conductivities have been measured in many nanostructures, including nanoporous materials<sup>8–14</sup>, nanowires<sup>15,16</sup> and thin films<sup>17</sup>, corroborating the use of such material systems for thermoelectric applications.

The thermoelectric figure-of-merit in semiconductors is defined as  $ZT = \sigma S^2 T / \kappa$ , where  $\sigma$  is the electrical conductivity,  $S$  is the Seebeck coefficient,  $\kappa$  is the lattice thermal conductivity and  $T$  the temperature. The numerator of  $ZT$  (the “power factor”) is generally maximized at relatively high carrier concentrations, so that the average electron MFP is on the order of a few nanometers<sup>18</sup>. Consequently, a properly engineered nanostructure can significantly decrease  $\kappa$  with little effect on  $\sigma$ , yielding an increase in  $ZT$ . Despite many attempts at minimizing thermal transport in nanostructures, however, thermal transport optimization is still largely unexplored, primarily due to practical experimental limitations and a lack of systematic engineering approaches.

In this work, we address the latter by introducing a novel concept, the directional phonon suppression function  $S(\Lambda, \Omega)$ , that describes the suppression of phonons with a given MFP  $\Lambda$  and direction within arbitrary geometries. By taking into account phonons travelling both along straight lines and through multiple phonon-boundary scattering events,  $S(\Lambda, \Omega)$  turns out to be a powerful tool for tuning thermal transport in complex nanostructures. We employ this approach to optimize thermal transport in Si-based nanoporous materials. We first compute the

Department of Mechanical Engineering, Massachusetts Institute of Technology, 77 Massachusetts Avenue, Cambridge, MA, 02139, USA. Correspondence and requests for materials should be addressed to G.R. (email: romanog@mit.edu)

thermal conductivity,  $\kappa$ , of a material system composed of a circular pores in a square lattice, finding significant heat transport degradation with respect to the bulk. Then, we use the information provided by  $S(\Lambda, \Omega)$  to identify a new structure, based on rectangular pores, that exhibits  $\kappa$  as small as  $1 \text{ Wm}^{-1}\text{K}^{-1}$ , well below the amorphous silicon limit ( $1.8 \text{ Wm}^{-1}\text{K}^{-1}$ )<sup>19</sup>. As our engineering approach can be applied to any combination of material and geometry, it paves the way to high-throughput search of ultra-low thermal conductivity materials.

## Bulk

While the methodology developed in this work is applicable to nanostructures with arbitrary materials and shapes, for the sake of clarity we describe our model specifically in relation to porous Si. The first step for computing heat transport in the presence of nanoscale boundaries is calculation of the thermal conductivity of the corresponding bulk material, which we denote  $\kappa_{bulk}$ . With no loss of generality, throughout the text we consider an isotropic bulk MFP distribution of a thermally isotropic material,  $K_{bulk}(\Lambda)$ , which is related to  $\kappa_{bulk}$  via

$$\kappa_{bulk} = 3 \int_0^\infty K_{bulk}(\Lambda) \langle \hat{\mathbf{s}}(\Omega) \otimes \hat{\mathbf{s}}(\Omega) \rangle_{4\pi} d\Lambda, \quad (1)$$

where  $\langle f(\Omega) \rangle_{4\pi}$  is the angular average  $(4\pi)^{-1} \int_{4\pi} f(\Omega) d\Omega$  and  $\hat{\mathbf{s}}(\Omega)$  is a versor described in terms of the polar angle  $\phi$  and the azimuthal angle  $\theta$ ,

$$\hat{\mathbf{s}}(\Omega) = \sin\theta \sin\phi \hat{\mathbf{x}} + \sin\theta \cos\phi \hat{\mathbf{y}} + \cos\theta \hat{\mathbf{z}}. \quad (2)$$

As  $\langle \hat{\mathbf{s}}(\Omega) \otimes \hat{\mathbf{s}}(\Omega) \rangle_{4\pi} = (1/3)\delta_{ij}$ , Eq. 1 reduces to the well-known formula  $\kappa_{bulk} = \int_0^\infty K_{bulk}(\Lambda) d\Lambda$ . The term  $K_{bulk}(\Lambda)$  is calculated via density functional theory<sup>6,7</sup>; for Si at room temperature, we obtain  $\kappa_{bulk} \approx 155 \text{ Wm}^{-1}\text{K}^{-1}$ , in agreement with previous work<sup>20</sup>.

## Macroscopic Limit

In porous materials, the volume removal has a degrading effect on heat flow. Furthermore, if the characteristic length  $L_c$  of the structure is comparable with the MFPs of heat-carrying phonons, size effects take place and the thermal conductivity is further suppressed. In order to compute the “effective” thermal conductivity  $\kappa$  (which is now a scalar) of an array of aligned pores, we identify a square unit-cell with size  $L$  containing a single pore, which is chosen to be circular, and apply a difference of temperature  $\Delta T$  along  $\hat{\mathbf{x}}$ , as shown in Fig. 1(a). Periodic boundary conditions are applied at the boundary of the unit cell. We consider the unit cell sizes  $L = 10 \text{ nm}$  and  $L = 50 \text{ nm}$ , keeping the diameter of the pore fixed so that the porosity of the material is  $\phi = 0.25$ . Assuming the heat flux,  $\mathbf{J}(\mathbf{r})$ , is known, we use Fourier’s law, i.e.,

$$\kappa = \frac{L}{\Delta T} \langle \mathbf{J}(\mathbf{r}) \rangle_{A_{hot}} \cdot \hat{\mathbf{n}}, \quad (3)$$

where  $\langle f(\mathbf{r}) \rangle_{A_{hot}} = A_{hot}^{-1} \int_{A_{hot}} f(\mathbf{r}) dS$  is an average along the surface of the hot contact and  $\hat{\mathbf{n}}$  is normal to this surface. We note that the thermal conductivity is now a scalar. For structures in which phonon-size effects are negligible, heat transport can be modelled by the heat diffusion equation, described by the heat flux  $\mathbf{J}(\mathbf{r}) = -\kappa_{bulk} \nabla T_L(\mathbf{r})$ , where  $T_L(\mathbf{r})$  is the spatially dependent lattice temperature, computed by the continuity equation  $\nabla \cdot \mathbf{J}(\mathbf{r}) = 0$ . Using Eq. 3, we obtain the general expression for the thermal conductivity reduction,

$$\frac{\kappa}{\kappa_{bulk}} = - \frac{L}{\Delta T} \nabla \langle T_L(\mathbf{r}) \rangle_{A_{hot}} \cdot \hat{\mathbf{n}}. \quad (4)$$

For porous materials with low porosity, macroscopic heat reduction is predicted by the Maxwell-Garnett theory which provides the formula  $\kappa/\kappa_{bulk} = (1 - \phi)/(1 + \phi) \approx 93 \text{ Wm}^{-1}\text{K}^{-1}$ <sup>21</sup>, in excellent agreement with our finite-volume solver of diffusive heat conduction.

## Directional Phonon Suppression Function

In aligned porous materials, the characteristic length  $L_c$  is roughly the pore-pore distance<sup>22</sup>, which in our cases is much shorter than the MFP of most of the dominant phonons in Si<sup>6</sup>, giving rise to significant phonon size effects. In order to take into account these effects, we employ the recently developed MFP-Boltzmann Transport Equation (MFP-BTE)<sup>23</sup>,

$$\Lambda \hat{\mathbf{s}}(\Omega) \cdot \nabla T(\mathbf{r}, \Lambda, \Omega) + T(\mathbf{r}, \Lambda, \Omega) = T_L(\mathbf{r}), \quad (5)$$

where  $T(\mathbf{r}, \Lambda, \Omega)$  is the effective temperature of phonons with MFP  $\Lambda$  and direction  $\hat{\mathbf{s}}(\Omega)$  and  $T_L(\mathbf{r})$  is the effective lattice temperature, given by

$$T_L(\mathbf{r}) = \frac{1}{4\pi} \int_0^\infty \int_{4\pi} A(\Lambda') T(\mathbf{r}, \Lambda', \Omega') d\Omega' d\Lambda'. \quad (6)$$

The weights  $A(\Lambda')$  ensure energy conservation and are expressed as

$$A(\Lambda') = \left[ \int \frac{K_{bulk}(\Lambda'')}{\Lambda''^2} d\Lambda'' \right]^{-1} \frac{K_{bulk}(\Lambda')}{\Lambda'^2}. \quad (7)$$

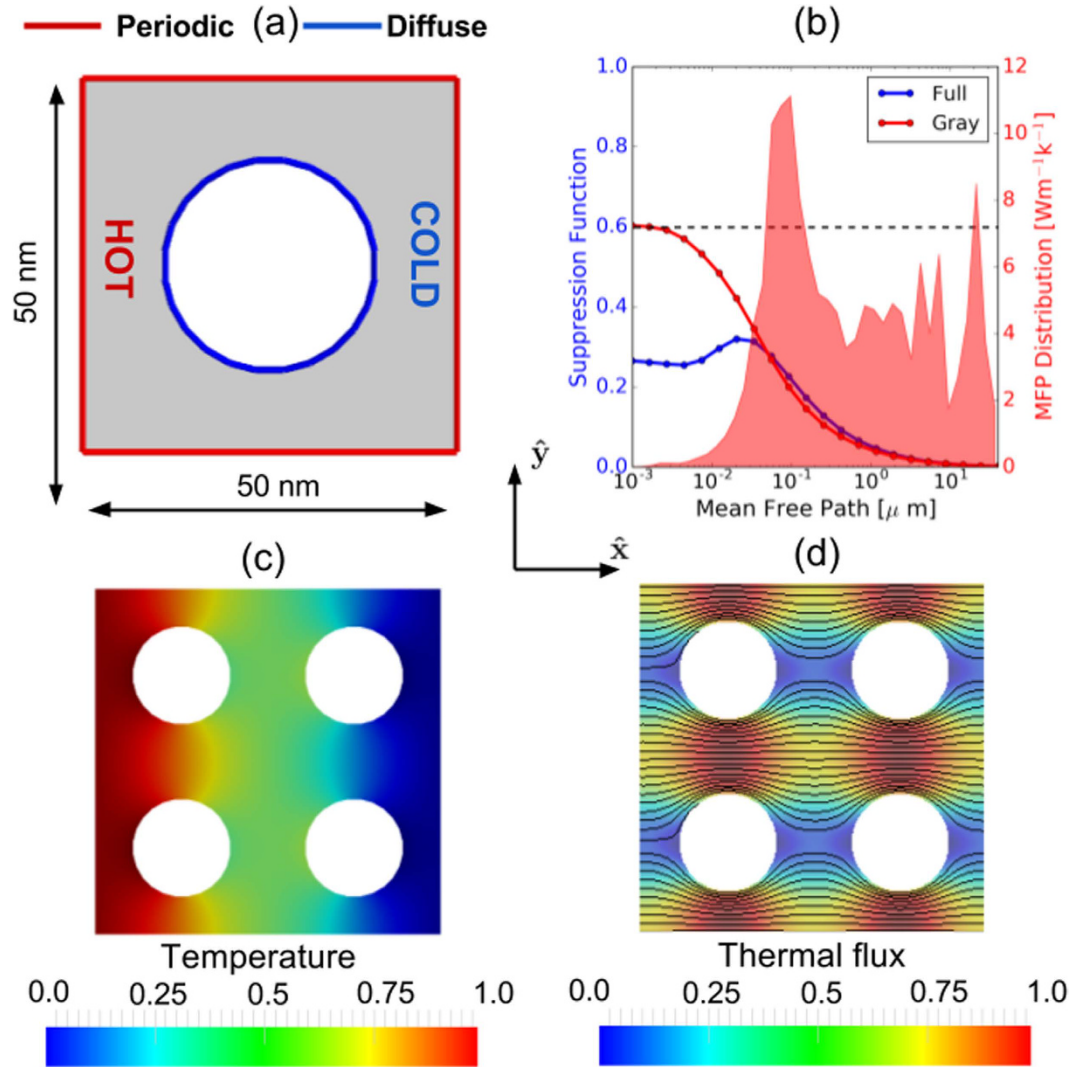


**Figure 1.** (a) Unit-cell comprising a single circular pore. The walls of the pores scatter phonons diffusively. Periodic boundary conditions are applied along both  $x$ - and  $y$ - directions. (b) Angular average of the directional phonon suppression for different MFPs, for both the gray model and the BTE described by Eq. 5. (c) Effective temperature distribution normalized to its maximum value. (d) Normalized magnitude of thermal flux superimposed to flux lines.

Similarly to ref. 24, the walls of the pores are assumed to scatter phonons diffusively. Further details about the computational approach are reported in the Methods section.

Once Eq. 5 is solved, we include the dependence on  $\Lambda$  and  $\Omega$  in Eq. 3 to compute the MFP distribution in the nanostructure, i.e.,

$$K_{nano}(\Lambda, \Omega) = \frac{L}{\Delta T} \langle \mathbf{J}(\mathbf{r}, \Lambda, \Omega) \rangle_{A_{hot}} \cdot \hat{\mathbf{n}}, \tag{8}$$

where

$$\mathbf{J}(\mathbf{r}, \Lambda, \Omega) = 3 \frac{K_{bulk}(\Lambda)}{\Lambda} T(\mathbf{r}, \Lambda, \Omega) \hat{\mathbf{s}}(\Omega) \tag{9}$$

is the thermal flux in the porous material<sup>23</sup>. After substituting Eqs 5–9 into Eq. 8, we obtain the following relationship

$$\frac{K_{nano}(\Lambda, \Omega)}{K_{bulk}(\Lambda)} - 3 \frac{L}{\Delta T \Lambda} \langle T_L(\mathbf{r}) \rangle_{A_{hot}} \hat{\mathbf{s}}(\Omega) \cdot \hat{\mathbf{n}} = S(\Lambda, \Omega), \tag{10}$$

where  $S(\Lambda, \Omega)$  is the “directional phonon suppression function”, given by

$$S(\Lambda, \Omega) = -3\frac{L}{\Delta T}\hat{\mathbf{s}}(\Omega) \otimes \hat{\mathbf{s}}(\Omega) \nabla \langle T(\mathbf{r}, \Lambda, \Omega) \rangle_{A_{\text{hot}}} \cdot \hat{\mathbf{n}}. \quad (11)$$

The directional phonon suppression function  $S(\Lambda, \Omega)$  is central to our work and describes the MFP dependence and directionality of phonon suppression caused by the boundaries. Once  $S(\Lambda, \Omega)$  is known, the thermal conductivity in the nanostructure is given by

$$\kappa = \int_0^\infty K_{\text{bulk}}(\Lambda) \langle S(\Lambda, \Omega) \rangle_{4\pi} d\Lambda. \quad (12)$$

The physical meaning of  $S(\Lambda, \Omega)$  can be better understood if we apply an angular average to both sides of Eq. 10, which gives

$$\langle S(\Lambda, \Omega) \rangle_{4\pi} = \frac{\langle K_{\text{nano}}(\Lambda, \Omega) \rangle_{4\pi}}{K_{\text{bulk}}(\Lambda)}, \quad (13)$$

where we used  $\langle \hat{\mathbf{s}}(\Omega) \cdot \hat{\mathbf{n}} \rangle_{4\pi} = 0$ . The term  $\langle S(\Lambda, \Omega) \rangle_{4\pi}$  is also given by

$$\langle S(\Lambda, \Omega) \rangle_{4\pi} = -\frac{L}{\Delta T} \nabla \langle \langle T(\mathbf{r}, \Lambda, \Omega) \rangle_{4\pi} \rangle_{A_{\text{hot}}} \cdot \hat{\mathbf{n}}, \quad (14)$$

which is the conventional MFP-dependent suppression function. This quantity, also called “boundary scattering”, is proven to be effective in MFP-reconstruction experiments and for understanding heat transport regime<sup>25–27</sup>. We note that the variable  $\Lambda$  is the bulk MFP; any result of this work can be translated in terms of the MFP in the nanostructure,  $\Lambda_{\text{nano}}$ , by means of the transformation  $\Lambda_{\text{nano}} = \Lambda \langle S(\Lambda, \Omega) \rangle_{4\pi}$ .

### Diffusive Limit

In the following section, we derive the diffusive and ballistic limits of  $S(\Lambda, \Omega)$  and connect the findings with the heat transport regimes of  $\langle S(\Lambda, \Omega) \rangle_{4\pi}$ . For short MFPs,  $T(\mathbf{r}, \Lambda, \Omega)$  can be expanded up to first-order spherical harmonics as ref. 28

$$T(\mathbf{r}, \Lambda, \Omega) = \langle T(\mathbf{r}, \Lambda, \Omega) \rangle_{4\pi} - \Lambda \hat{\mathbf{s}}(\Omega) \cdot \nabla \langle T(\mathbf{r}, \Lambda, \Omega) \rangle_{4\pi}. \quad (15)$$

Combining with Eq. 5, multiplying both sides by  $\hat{\mathbf{s}}$  and applying an angular average, this gives<sup>23,28</sup>

$$\frac{\Lambda^2}{3} \nabla^2 \langle T(\mathbf{r}, \Lambda, \Omega) \rangle_{4\pi} = \langle T(\mathbf{r}, \Lambda, \Omega) \rangle_{4\pi} - T_L(\mathbf{r}), \quad (16)$$

which is a modified heat diffusion equation that takes into account interactions among phonons with different MFPs. After combining Eqs 11–16, we obtain the diffusive limit of  $S(\Lambda, \Omega)$ ,

$$S(\Lambda \rightarrow 0, \Omega) = -3\frac{L}{\Delta T}\hat{\mathbf{s}}(\Omega) \otimes \hat{\mathbf{s}}(\Omega) \nabla \langle T(\mathbf{r}, \Lambda, \Omega) \rangle_{4\pi} \cdot \hat{\mathbf{n}} + 3\frac{L}{\Delta T\Lambda} \left( \langle T(\mathbf{r}, \Lambda, \Omega) \rangle_{4\pi} - T_L(\mathbf{r}) \right)_{A_{\text{hot}}} \hat{\mathbf{s}}(\Omega) \cdot \hat{\mathbf{n}}. \quad (17)$$

In Eq. 17, the second term represents the fact that the medium is non-gray. In fact, under the gray-medium approximation, where the lattice temperature is  $T_L(\mathbf{r}, \Lambda) = \langle T(\mathbf{r}, \Lambda, \Omega) \rangle_{4\pi}$ , this term vanishes. In this case, phonons are solved independently, leading to a MFP-dependent lattice temperature. For simplicity and with no loss in generality, we now derive the expression of  $S(\Lambda \rightarrow 0, \Omega)$  for our nanoporous system within the gray approximation. Under these assumptions, Eq. 16 becomes the Laplacian equation  $\nabla^2 T_L(\mathbf{r}) = 0$ , *i.e.*, the standard Fourier’s law<sup>29</sup>. By assuming a constant heat flux along the hot contact, the gradient of the lattice temperature is simply  $\nabla T_L(\mathbf{r}) \approx -f(\phi)(\Delta T/L)\hat{\mathbf{x}}$  and Eq. 11 then becomes

$$S^{\text{gray}}(\Lambda \rightarrow 0, \Omega) = 3f(\phi)\sin^2\theta \sin^2\varphi, \quad (18)$$

where we used  $\hat{\mathbf{n}} = \hat{\mathbf{x}}$ . The Cartesian representation of  $S(\Lambda \rightarrow 0, \Omega)$ , represented by the surface  $\mathbf{r}(\Omega) - S(\Lambda \rightarrow 0, \Omega)\hat{\mathbf{s}}(\Omega) = 0$ , is plotted in Fig. 2(a). We note two lobes, oriented along  $\hat{\mathbf{x}}$  and  $-\hat{\mathbf{x}}$ , consistently with the fact that both the direction of the applied temperature gradient and the normal of the cold contact are aligned with  $\hat{\mathbf{x}}$ . This symmetry can be also seen by the polar representation

$$S(\Lambda, \varphi) = \frac{1}{2} \int_0^\pi S(\Lambda, \varphi) \sin\theta d\theta, \quad (19)$$

which, when applied to Eq. 17, becomes  $S(\Lambda \rightarrow 0, \varphi) = 2f(\phi)\sin^2\varphi$ , as shown in Fig. 2(b). The diffusive limit of  $\langle S(\Lambda, \Omega) \rangle_{4\pi}$  within the gray approximation can be obtained by simply performing an angular average of the polar suppression function, *i.e.*

$$\langle S^{\text{gray}}(\Lambda \rightarrow 0, \Omega) \rangle_{4\pi} = \frac{1}{\pi} f(\phi) \int_0^{2\pi} \sin^2\varphi d\varphi = \frac{1-\phi}{1+\phi}, \quad (20)$$

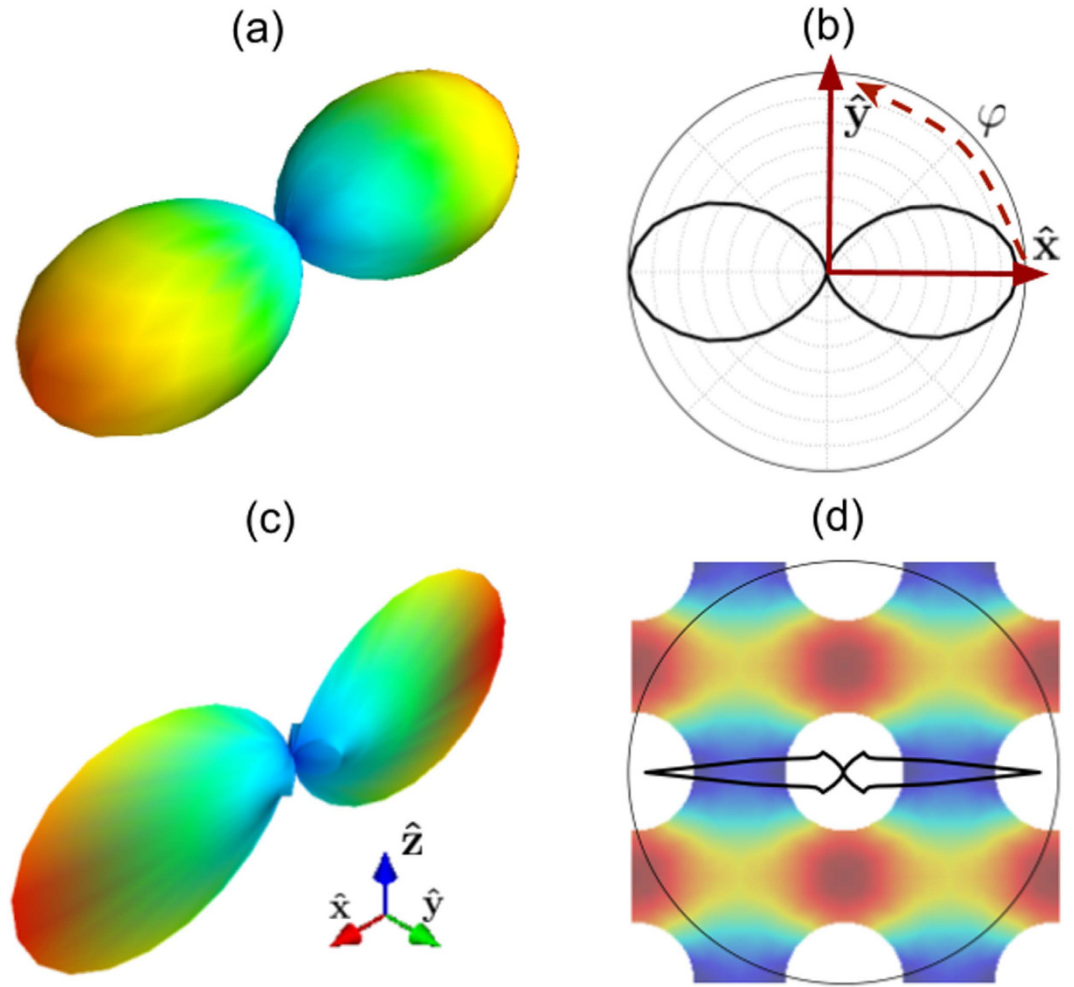


**Figure 2.** Spherical (a) and polar (b) representations of  $S(\Lambda, \Omega)$  for low  $Kn$ s. The two lobes are identical because of the system symmetry. (c) Spherical and (d) polar representation of  $S(\Lambda, \Omega)$  for high  $Kn$ s. The two lobes are peaked at  $\phi = 0$  and  $\phi = \pi$ . The periodicity is  $L = 50$  nm.

which is the value obtained by Fourier’s law, as shown in Fig. 1(b). However, by using the general expression for non-gray media from Eq. 14, we obtain a lower value for very small MFPs with a peak around 30 nm. This result suggests that the trend obtained by the full MFP-BTE is due to the interaction among phonons with different MFPs. Specifically, the discrepancy in  $\langle S(\Lambda, \Omega) \rangle_{4\pi}$  for low-MFP phonons between the gray and the non-gray models arises from the fact that diffusive phonons in Eq. 5 tend to thermalize to an effective temperature (plotted in Fig. 1(c)) that also depends on ballistic phonons.

**Ballistic Limit**

We now investigate the ballistic limit of  $S(\Lambda, \Omega)$ . For large MFPs, boundary scattering becomes predominant and  $S(\Lambda, \Omega)$  starts to depend strongly on the geometry of the material. In this regime, Eq. 5 becomes<sup>5</sup>

$$\hat{\mathbf{s}}(\Omega) \cdot \nabla T(\mathbf{r}, \Lambda, \Omega) = - \frac{T(\mathbf{r}, \Lambda, \Omega)}{\Lambda} \tag{21}$$

After combining Eqs 11–21, we have

$$\Lambda S(\Lambda \rightarrow \infty, \Omega) = 3 \frac{L}{\Delta T} \langle T(\mathbf{r}, \Lambda, \Omega) \rangle_{A_{\text{hot}}} \hat{\mathbf{s}}(\Omega) \cdot \hat{\mathbf{n}}, \tag{22}$$

which recovers the well-known behaviour  $S(\Lambda \rightarrow \infty, \Omega) \propto \Lambda^{-1}$  for the ballistic regime<sup>5</sup>. We note that in this case, the directional suppression function is simply the ratio between the MFP distribution in the nanostructure and that in the bulk, *i.e.*  $K_{\text{nano}}(\Lambda \rightarrow \infty, \Omega) = S(\Lambda \rightarrow \infty, \Omega) K_{\text{bulk}}(\Lambda)$ , and so applies to  $\langle S(\Lambda, \Omega) \rangle_{4\pi}$ . As shown in Fig. 2(c),  $S(\Lambda, \Omega)$  is pronounced for  $\phi = 0$  and  $\phi = \pi$ , whereas it rapidly vanishes for other polar angles. This trend can be explained in terms of the view factor, a geometric parameter that quantifies the possibility of having a direct path between the hot and cold contacts<sup>30</sup>. In porous materials with square pore lattices, most of the heat travels through the spaces between the pores, perpendicular to the applied temperature gradient. The relative contribution of

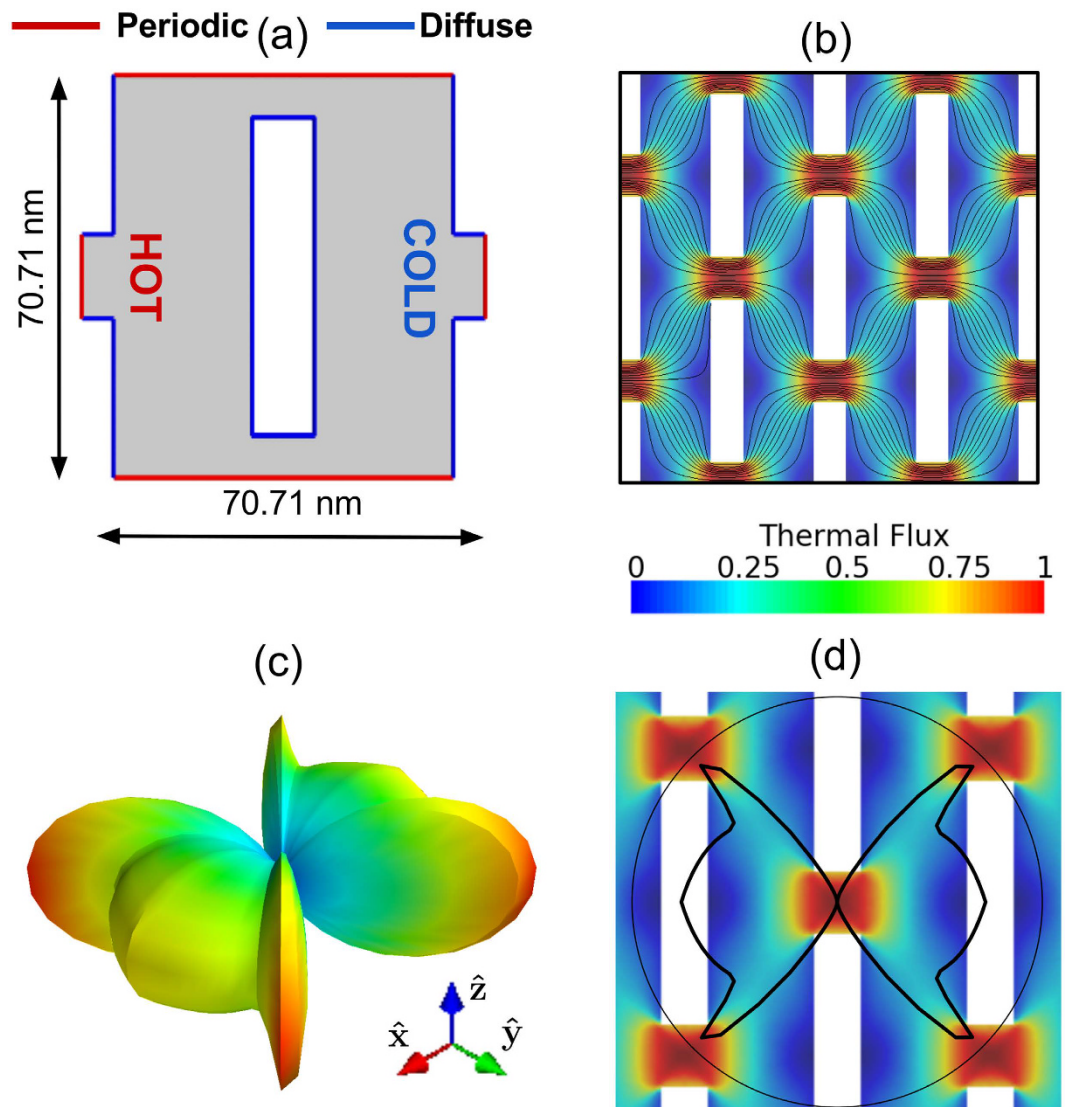


**Figure 3.** (a) Unit-cell of the configuration with staggered rectangular pores. (b) Normalized magnitude of thermal flux and flux lines. There are not direct paths from the cold to the hot side. (c) Spherical and (d) polar representation of  $S(\Lambda, \Omega)$ . All thermal transport arises from multiple phonon boundary scattering.

such paths is the view factor. Figure 2(d) superimposes  $S(\Lambda, \Omega)$  and the material geometry to better elucidate the relationship between the boundary arrangements and phonon suppression. We also note four sub-lobes corresponding to phonons travelling along directions at 45 degrees with respect to the applied temperature gradient, constituting another set of direct paths. For all the other directions,  $S(\Lambda, \Omega)$  describes Multiple Phonon-Boundary (MPB) scattering. In our case, heat transport arising from MPB is negligible, with most of the heat carried by phonons travelling through direct paths.

### Material Optimization

Using the insights from above, we identify a new nanopore geometry with the same porosity as the circular nanopore case, that has improved properties. This new geometry consists of rectangular pores in a staggered configuration, as shown in Fig. 3(a). The periodicity is larger than the previous case because of the fixed-porosity requirement. From the flux lines plotted in Fig. 3(b), we note that direct paths are absent; thus, phonons scatter multiple times before reaching the cold contact. For low  $Kn_s$ ,  $S(\Lambda, \Omega)$  is similar to that of the case with circular pores, with the size of the lobes determined by the porosity function  $f(\phi)$  of the new configuration. Interestingly, for high  $Kn_s$ ,  $S(\Lambda, \Omega)$  has six preferred directions, as shown in Fig. 3(d). The amplitudes of these peaks are significantly smaller than those in Fig. 2(d). Remarkably, the computed  $\kappa$  are  $4 \text{ Wm}^{-1}\text{k}^{-1}$  and  $1 \text{ Wm}^{-1}\text{k}^{-1}$  for  $L = 50 \text{ nm}$  and  $L = 10 \text{ nm}$ , respectively, almost five times smaller than their counterparts with circular pores. We note that, for the case with  $L = 10 \text{ nm}$ ,  $\kappa$  is smaller than that of amorphous silicon<sup>19</sup>. Finally, as this very low thermal conductivity is obtained with no change in the porosity, the transport of electrons, which travel diffusively, will not be significantly suppressed. As a result, the configuration with staggered rectangular pores has promise as a high-ZT material.

## Conclusions

In summary, we have introduced the directional phonon suppression function, a novel concept that captures the essence of size effects in unprecedented detail. Guided by this new quantity, we have identified a porous structure, based on rectangular pores arranged in a staggered configuration, with ultra-low thermal conductivity and relatively low porosity. Our work furthers the general understanding of boundary-dominated heat transport. In addition, as our approach is suitable for any combinations of material and geometry, this work provides practical guidance for the development of novel, high-efficiency thermoelectric materials.

## Method

The cumulative thermal conductivity requires the calculation of the three-phonon scattering time. These calculations were performed with a  $32 \times 32 \times 32$  grid in reciprocal space and a  $4 \times 4 \times 4$  supercell. Force constants calculations were performed with a  $5 \times 5 \times 5$  supercell. The isotope disorder scattering is included in the calculation. Phonon-related calculations were carried out using ShengBTE<sup>20</sup>. Density functional theory calculations were performed with Quantum Espresso<sup>31</sup>. Using a projected augmented wave (PAW) pseudopotential<sup>32</sup>, with a plane-wave cut-off of 320 meV, and a  $11 \times 11 \times 11$  k-point mesh. Phonon size effects were calculated using an in-house code. The spatial domain was discretized using the finite-volume method solved over an unstructured grid with approximately 6000 elements. The solid angle was discretized into 48 polar and 12 azimuthal angles. The material was assumed to be infinite along the  $z$ -direction. The MFP distribution, assumed to be isotropic, was discretized into 30 MFPs.

## References

- Rowe, D. M. (ed.) *CRC Handbook of Thermoelectrics* (CRC Press, Boca Raton, FL, 1995).
- Vineis, C., Shakouri, A., Majumdar, A. & Kanatzidis, M. Nanostructured thermoelectrics: big efficiency gains from small features. *Adv. Mater.* **22**, 3970–80 (2010).
- Li, B., Wang, L. & Casati, G. Thermal diode: rectification of heat flux. *Phys. Rev. Lett.* **93**, 184301 (2004).
- Lai, J. & Majumdar, A. Concurrent thermal and electrical modeling of submicrometer silicon devices. *J. Appl. Phys.* **79**, 7353–7361 (1996).
- Chen, G. *Nanoscale energy transport and conversion: a parallel treatment of electrons, molecules, phonons, and photons* (Oxford University Press, USA, 2005).
- Esfarjani, K., Chen, G. & Stokes, H. T. Heat transport in silicon from first-principles calculations. *Phys. Rev. B* **84**, 085204 (2011).
- Broido, D., Malorny, M., Birner, G., Mingo, N. & Stewart, D. Intrinsic lattice thermal conductivity of semiconductors from first principles. *Appl. Phys. Lett.* **91**, 231922 (2007).
- Song, D. & Chen, G. Thermal conductivity of periodic microporous silicon films. *Appl. Phys. Lett.* **84**, 687–689 (2004).
- Lee, J., Lim, J. & Yang, P. Ballistic phonon transport in holey silicon. *Nano Lett.* **15**, 3273 (2015).
- Tang, J. *et al.* Holey Silicon as an Efficient Thermoelectric Material. *Nano Lett.* **10**, 4279–4283 (2010).
- Hopkins, P. E. *et al.* Reduction in the Thermal Conductivity of Single Crystalline Silicon by Phononic Crystal Patterning. *Nano Lett.* **11**, 107–112 (2011).
- Kargar, F. *et al.* Acoustic phonon spectrum and thermal transport in nanoporous alumina arrays. *Appl. Phys. Lett.* **107**, 171904 (2015).
- De Boor, J. *et al.* Temperature and structure size dependence of the thermal conductivity of porous silicon. *EPL* **96**, 16001 (2011).
- Vega-Flick, A. *et al.* Thermal transport in suspended silicon membranes measured by laser-induced transient gratings. *AIP Adv.* **6**, 121903 (2016).
- Boukai, A. I. *et al.* Silicon nanowires as efficient thermoelectric materials. *Nature* **451**, 168–171 (2008).
- Hochbaum, A. I. *et al.* Enhanced thermoelectric performance of rough silicon nanowires. *Nature* **451**, 163–167 (2008).
- Venkatasubramanian, R., Siivola, E., Colpitts, T. & O'Quinn, B. Thin-film thermoelectric devices with high room-temperature figures of merit. *Nature* **413**, 597–602 (2001).
- Liao, B. *et al.* Significant reduction of lattice thermal conductivity by the electron-phonon interaction in silicon with high carrier concentrations: A first-principles study. *Phys. Rev. Lett.* **114**, 115901 (2015).
- Wada, H. & Kamijoh, T. Thermal conductivity of amorphous silicon. *Jpn. J. Appl. Phys.* **35**, L648 (1996).
- Li, W., Carrete, J., A. Katcho, N. & Mingo, N. ShengBTE: A solver of the boltzmann transport equation for phonons. *Comput. Phys. Commun.* **185**, 1747–1758 (2014).
- Nan, C., Birringer, R., Clarke, D. R. & Gleiter, H. Effective thermal conductivity of particulate composites with interfacial thermal resistance. *J. Appl. Phys.* **81**, 6692–6699 (1997).
- Romano, G. & Grossman, J. C. Toward phonon-boundary engineering in nanoporous materials. *Appl. Phys. Lett.* **105**, 033116 (2014).
- Romano, G. & Grossman, J. C. Heat conduction in nanostructured materials predicted by phonon bulk mean free path distribution. *J. Heat Transf.* **137**, 071302 (2015).
- Romano, G., Esfarjani, K., Strubbe, D. A., Broido, D. & Kolpak, A. M. Temperature-dependent thermal conductivity in silicon nanostructured materials studied by the boltzmann transport equation. *Phys. Rev. B* **93**, 035408 (2016).
- Minnich, A. J. *et al.* Thermal conductivity spectroscopy technique to measure phonon mean free paths. *Phys. Rev. Lett.* **107**, 095901 (2011).
- Yang, F. & Dames, C. Mean free path spectra as a tool to understand thermal conductivity in bulk and nanostructures. *Phys. Rev. B* **87** (2013).
- Minnich, A. J. Thermal phonon boundary scattering in anisotropic thin films. *Appl. Phys. Lett.* **107**, 183106 (2015).
- Chen, G. Ballistic-diffusive heat-conduction equations. *Physical Review Letters* **86**(11), 2297 (2001).
- Ziman, J. *Electrons and Phonons* (Oxford University Press (OUP), 2001).
- Prasher, R. Thermal conductivity of composites of aligned nanoscale and microscale wires and pores. *J. Appl. Phys.* **100**, 034307 (2006).
- Giannozzi, P. *et al.* QUANTUM ESPRESSO: a modular and open-source software project for quantum simulations of materials. *J. Phys. Condens. Matter* **21**, 395502 (2009).
- Blöchl, P. E. Projector augmented-wave method. *Phys. Rev. B Condens. Matter* **50**, 17953–17979 (1994).

## Acknowledgements

Research supported as part of the Solid-State Solar-Thermal Energy Conversion Center (S3TEC), an Energy Frontier Research Center funded by the US Department of Energy (DOE), Office of Science, Basic Energy Sciences (BES), under Award DESC0001.

### Author Contributions

G.R. performed all calculations. G.R. and A.M.K. analyzed and interpreted the data and prepared the manuscript.

### Additional Information

**Competing Interests:** The authors declare no competing financial interests.

**How to cite this article:** Romano, G. and Kolpak, A. M. Directional Phonon Suppression Function as a Tool for the Identification of Ultra-Low Thermal Conductivity Materials. *Sci. Rep.* **7**, 44379; doi: 10.1038/srep44379 (2017).

**Publisher's note:** Springer Nature remains neutral with regard to jurisdictional claims in published maps and institutional affiliations.



This work is licensed under a Creative Commons Attribution 4.0 International License. The images or other third party material in this article are included in the article's Creative Commons license, unless indicated otherwise in the credit line; if the material is not included under the Creative Commons license, users will need to obtain permission from the license holder to reproduce the material. To view a copy of this license, visit <http://creativecommons.org/licenses/by/4.0/>

© The Author(s) 2017